# Atomistic simulation of energetic and entropic elasticity in short-chain polyethylenes

T. C. Ionescu

*Department of Chemical Engineering, University of Tennessee,*
*Knoxville, Tennessee 37996*

V. G. Mavrantzas

*Department of Chemical Engineering, University of Patras and*
*Institute of Chemical Engineering and High Temperature Chemical Processes*
*(FORTH-ICE/HT), Patras GR 26504, Greece*

D. J. Keffer and B. J. Edwards[a]

*Department of Chemical Engineering, University of Tennessee,*
*Knoxville, Tennessee 37996*

## Synopsis

The thermodynamical aspects of polymeric liquids subjected to uniaxial elongational flow are examined using atomistically detailed nonequilibrium Monte Carlo simulations. In particular, attention is paid to the energetic effects, in addition to the entropic ones, which occur under conditions of extreme deformation. Atomistic nonequilibrium Monte Carlo simulations of linear polyethylene systems, ranging in molecular length from $C_{24}$ to $C_{78}$ and for temperatures from 300 to 450 K, demonstrate clear contributions of energetic effects to the elasticity of the system. These are manifested in a conformationally dependent heat capacity, which is significant under large deformations. Violations of the hypothesis of purely entropic elasticity are evident in these simulations, in that the free energy of the system is demonstrated to be composed of significant energetic effects under high degrees of orientation. These arise mainly from favorable intermolecular side-to-side interactions developing in the process of elongation due to chain uncoiling and alignment in the direction of extension. © *2008 The Society of Rheology.* [DOI: 10.1122/1.2838250]

## I. INTRODUCTION

Polymer elasticity is related to the ability of chains to sustain or accommodate large deformations through rearrangement of their configurations. Rubber-like elasticity, in particular, is related to the ability of a material to sustain deformations up to five or ten times its unstretched length without rupture. It is also related to the development of a restoring force as the rubbery material deforms, which gives it the capacity to recover

---

[a]Author to whom correspondence should be addressed; electronic mail: bje@utk.edu

J. Rheol. 52(2), 567-589 March/April (2008)     0148-6055/2008/52(2)/567/23/$27.00     567

(practically instantaneously) its original dimensions. As stated by Flory (1953), the presence of long chains is a necessary condition for rubber-like behavior but not a sufficient one, since the system should also possess sufficient internal mobility to allow the required rearrangements of chain configurations during deformation and relaxation.

To describe rubber-like elasticity, classical molecular theories have been based on an important postulate, namely, that elasticity is an intramolecular property; any intermolecular interactions are considered to be independent of the extent of deformation. Therefore, these interactions should play no role in deformations carried out at constant volume. A second postulate separates the Helmholtz free energy of the elastic network into liquid-like inelastic and elastic contributions, the latter depending on an appropriately defined strain tensor.

In general, when a polymer system that is neither fully crystalline nor in the glassy state is subjected to an externally applied stress, a large deformation can be accommodated through uncoiling of the chains and their orientation parallel to the axis of elongation. In network models, the chains are ordinarily connected to one another at the junction points. In rubbery solids, these are permanent cross linkages, whereas in macromolecular fluids these are viewed as temporary physical entanglements or topological constraints. In recent theories, such as those based on principles of nonequilibrium thermodynamics, chain segments between such physical entanglements are explicitly used as state variables in the system description through the definition of a connector vector which, at equilibrium, is routinely assumed to obey Gaussian statistics. To account for intermediate microscopic configurations in a nonequilibrium process, use is often made of a more global variable, namely, the conformation tensor corresponding to the second moment of the distribution function for the connector vector.

The concept of the conformation tensor (or, equivalently, of an appropriately defined strain tensor) is central to theories of irreversible thermodynamics of polymer elasticity and viscoelasticity, where a generalized expression is invoked for the Helmholtz free energy, $A$, of the system. Mapping out $A$ in terms of molecular variables (such as the conformation tensor or the strain tensor) is an outstanding issue in the polymer science community, which has been examined over the years using either theoretical or computational techniques. From the perspective of a simulationist, in particular, it is evident that overly long simulation times (on the order of tens of microseconds) are required to sample the dynamic information necessary to link macroscopic thermodynamics and molecular properties. This is due to the huge gap between time and length scales between the motions of polymer segments and flow in melt processing operations. Alternatively, if one is interested only in the steady-state configurational and thermodynamic properties of the deformed system, then this problem can be overcome through the design of static methods, such as the field-on Monte Carlo approach proposed by Mavrantzas and Theodorou (1998) and Mavrantzas and Öttinger (2002).

By postulating the free energy to have an extra dependence on the conformation tensor, such an approach allows one to calculate the elasticity of a polymer melt through thermodynamic integration at progressively higher values of an orienting tensorial field, the conjugate thermodynamic variable to the conformation tensor. This method was applied to simulations of two short-chain polyethylene (PE) liquids, $C_{24}H_{50}$ and $C_{78}H_{158}$, at a temperature $T = 450$ K, which were subjected to a static orienting field that was postulated to produce the same effect as the homogeneous, one-dimensional extensional flow at constant strain rate [Mavrantzas and Theodorou (1998, 2000)].

As discussed in a recent Letter [Baig and Mavrantzas (2007)] designing a methodology in order to drive an ensemble of system configurations to sample appropriate nonequilibrium phase-space points corresponding to an imposed flow is not a trivial issue.

The correspondence between an externally applied static field and a real flow cannot be exact, because, for example, the kinetic degrees of freedom and their coupling to the configurational degrees of freedom are neglected in nondynamic simulations. Assigning a clear kinematic interpretation to the synthetic forces employed in Monte Carlo simulations (through the use of a static field) in terms of the true velocity gradient tensor applied in shear and elongational flows is not always possible. It is not surprising therefore that the first attempts to apply field-on Monte Carlo methodologies to study the flow deformation of polymers were made for the case of homogeneous extensional flow at constant elongation rate in one direction, since such a flow has the simplest kinematical structure in nonequilibrium Monte Carlo simulations of flowing systems. A key result of the earlier works by Mavrantzas and Theodorou (1998, 2000) was that the response of the system to the applied field is entropic only at small values of the imposed field. In contrast, a significant energetic component develops for larger values of the imposed elongational field due to the development of favorable lateral atom-atom interactions. Unfortunately, due to lack of computational resources at the time, only the $C_{24}H_{50}$ PE liquid was thoroughly investigated over a broad enough range of field values up to the point where full chain extension takes place. For the longer $C_{78}H_{158}$ liquid, the analysis was restricted to relatively small elongational fields, for which the response of the system was observed to be always purely entropic.

It is the purpose of this paper to enlarge the prior analysis by carrying out a more extensive suite of simulations for a larger number of PE liquids (from $C_{24}H_{50}$ to $C_{78}H_{158}$) and a broader range of elongational rates, including thermal effects. Section II gives an outline of the basic principles of the theoretical approach to polymer elasticity. Section III presents the simulation method (nonequilibrium Monte Carlo) employed to study oriented polymer melts and their elasticity. This section contains a review of the thermodynamic and statistical mechanical formulation underlying the work, introduces the molecular model, and explains the computational methodology for simulating polymer chain elasticity. Section IV presents results for the energetic contribution to the free energy of a number of short-chain polyethylene liquids, including its separation into intramolecular and intermolecular components. Section V summarizes the most important conclusions of this study.

## II. THEORETICAL BACKGROUND

The Helmholtz free energy is defined as the Legendre transform of the internal energy,

$$A \equiv U - TS. \tag{1}$$

The hypothesis of purely entropic elasticity assumes that the free energy change under an applied strain is governed entirely by the entropic configurational response of the chains to deformation [Astarita (1974); Astarita and Sarti (1976a, 1976b); Sarti *et al.* (1977)].

In general, polymer melts and nondilute solutions display a significant degree of elasticity. Recent advances in atomic force microscopy have made it possible to measure the mechanical properties of polymers at the molecular level. Consequently, a considerable amount of effort has been dedicated to measuring the elastic responses of single polymer chains in various media [Ortiz and Hadziioannou (1999); Lu *et al.* (2004); Nakajima *et al.* (2006); Shi *et al.* (2006)]. The general consensus is that when single polymer chains are extended, their elastic response can be attributed entirely to a decrease in conformational entropy. A recent molecular simulation study appeared to substantiate this notion [Bedrov and Smith (2003); Smith *et al.* (2005)]. In this study, the authors measured the elastic response of a single chain placed in a simulation box, which was

filled with a solvent (either chemically different or similar to the single chain). The authors then proceeded to extend the chain and map out its free energy using the "umbrella sampling" technique, while keeping the surrounding solvent at equilibrium. They concluded that, unless the chain reaches its maximum extension length, the internal energy of the system does not change. By definition, the chain adopts its maximum extension when all the torsional angles are in the *trans* conformation, while the bond angles and bond lengths are at their equilibrium values. Clearly, the internal energy increase observed at the highest extensions was due to modifications in bond angles.

As to be demonstrated in Sec. III, the present simulation results suggest that when a polymer melt (or an ensemble of chains) is stretched, the most important contributor to the change in internal energy is the intermolecular nonbonded energy. The two other major contributors are the torsional energy and the intramolecular nonbonded energy, which are of about the same magnitude but opposite in sign, thereby largely canceling each other. Therefore, the results obtained by single-chain elasticity measurements are not at all surprising, since the medium surrounding the extended polymer chain was kept at equilibrium; thus the change in the nonbonded intermolecular energy was negligible. In reality, when a polymeric liquid experiences deformation, the macromolecular chains tend to align relative to the direction of the deformation, establishing more favorable side-side interactions with the neighboring chains. This plays a major role in the energy balance of the system, because these favorable interactions lower the intermolecular nonbonded energy significantly. In extreme cases, the oriented melts experience the phenomenon called "flow-induced crystallization." Indeed, evidence has been presented previously of crystalline-like precursor structures forming during simulation of n-eicosane subjected to planar elongational flow [Ionescu *et al.* (2006)].

If we examine the internal structure of cross-linked rubbery solids, the chain segments connecting two network nodes can be modeled as isolated chains. When an external deformation is applied, it is very difficult for the chain segments to establish favorable side-side interactions with neighboring chains, given the random distribution of the network nodes and the segment lengths. Thus, the intermolecular interactions will be independent of deformation. Therefore, the energy accumulated through deformation will be primarily associated with a decrease in configurational entropy, as discussed by Treloar (1975).

Astarita and co-workers [Astarita (1974); Astarita and Sarti (1976a, 1976b); Sarti and Esposito (1977)] set the basis for what it is known today as the Theory of *Purely Entropic Elasticity* (PEE) as applied to polymer melts. They have made the assumption that the internal energy of a polymeric fluid is a unique function of temperature, and thus independent of deformation. This assumption is the same as that used to describe many aspects of cross-linked rubbers, in that the entire free energy change under deformation is attributed to entropic effects. Mathematically, this assumption is expressed as

$$\hat{U} = \hat{U}(T) \tag{2}$$

and the immediate consequence of this functional relationship is that the constant volume heat capacity per unit mass, defined in the usual fashion as the derivative of the internal energy with respect to temperature at constant density, will also be independent of deformation,

$$\hat{c}_v = \frac{\mathrm{d}\hat{U}(T)}{\mathrm{d}T}. \tag{3}$$

The most widely used quantity to describe the internal structure of linear polymer

melts is the conformation tensor, **c**, which is defined as the second moment (dyadic product) of the end-to-end vector, **R**, taken as an ensemble average,

$$\mathbf{c} \equiv \langle \mathbf{RR} \rangle. \tag{4}$$

If we consider both temperature and conformation tensor functionalities of the internal energy (for an incompressible fluid),

$$\hat{U} = \hat{U}(T, \mathbf{c}), \tag{5}$$

then the constant volume heat capacity per unit mass will be defined as the partial derivative of the internal energy with respect to temperature at constant **c**,

$$\hat{c}_v = \left. \frac{\partial \hat{U}}{\partial T} \right|_{\mathbf{c}}. \tag{6}$$

Using the free energy expression of Booij (1984), which is the underlying basis of many common rheological models such as the Upper-Convected Maxwell Model and the Giesekus Model, the heat capacity can be expressed as a sum of two terms: the equilibrium heat capacity, $\hat{c}_0$, and an explicit contribution from the conformational structure of the polymer [Dressler *et al.* (1999)],

$$\hat{c}_v = \hat{c}_0 - \frac{1}{2} \gamma T (\mathrm{tr}\mathbf{c} - \mathrm{tr}\mathbf{c}_0) \frac{\partial^2 K(T)}{\partial T^2}. \tag{7}$$

In this expression, $\gamma$ is a material constant related to the degree of elasticity per unit mass, $K(T)$ is the (temperature-dependent) overall chain Hookean spring constant, **c** is the conformation tensor in the deformed state, and $\mathbf{c}_0$ is the conformation tensor in the unperturbed state. This expression was derived assuming the Booij free energy expression [Booij (1984)], and if $K(T)$ is a linear function of temperature, the second term on the right side of Eq. (7) vanishes. However, as we shall see later in Sec. IV, the simulation results demonstrate that $K(T)$ is not a linear function of temperature, and the conformational contribution to the heat capacity may thus be significant at large deformations. Furthermore, it is worth emphasizing that the functional form of Eq. (7) is based upon the relatively simplistic free energy expression of Booij. Other free energy expressions, such as the one corresponding to the Finitely Extensible Nonlinear Elastic Spring Model [Beris and Edwards (1990a, 1990b, 1994)], would produce different functional forms for this thermophysical property. It should also be mentioned that for nonlinear polymers, e.g., for the branched H-shaped polymer structure, the use of a single conformation tensor is not sufficient to describe their response to an applied flow field. For these more complex architectures, one should use two variables: the branch-to-branch point traceless orientation tensor, **S**, and a scalar variable, λ, accounting for deformations in the length of the branch segments. In general, given a polymeric liquid with a particular molecular architecture, it is not always straightforward to define the appropriate coarse-grained structural variables to describe the response to a flow field; in some cases, there must be more than one way through which this can be done. For example, Bernardin and Rutledge (2007) have studied the viscoelasticity of linear polymers, not by using the conformation tensor as the appropriate structural variable, but the bond order parameter corresponding to the 2nd Lagrange polynomial. In general, in the selection of the most appropriate structural variables to describe systems beyond equilibrium, it is important that one is guided by a macroscopic viscoelastic model with proven thermodynamic admissibility [Beris and Edwards (1994); Öttinger (2005)].

The heat capacity represents the amount of heat necessary to raise the temperature of a unit mass of an object by one degree Kelvin. This amount of heat is directly related to the degrees of freedom of the smallest components (atoms) of that particular object. When a polymeric material is subjected to deformation, the macromolecular chains align on average relative to the direction of the deformation, which results in a decrease of the available configurations of the chains; in other words, a reduction in the heat capacity. Therefore, one would expect that the heat capacity for an aligned system of macromolecules would always be smaller than the quiescent state value. Indeed, as demonstrated later in Sec. III, the heat capacity decreases as the deformation rate increases for the model polymer (polyethylene) studied in this article.

## III. MOLECULAR SIMULATION OF ORIENTED POLYMER MELTS

From an experimental perspective, studying the structure-property relationships in a polymeric material is not always an easy task. Over the past three decades, computer simulation techniques have developed as useful tools to aid researchers in understanding many issues concerning the dynamic, structural, and thermodynamic properties of physical systems.

In general, relatively small systems are sufficient to generate thermodynamic properties of small molecular weight compounds. This is not the case for polymeric liquids. Unlike small molecule compounds, polymers exhibit a wide spectrum of time and length scales characterizing their dynamic behavior and internal structure; this is the source of many challenges to be overcome when simulating polymeric materials. With the rapid advancements of computational hardware and the development of new, efficient algorithms, molecular simulation of polymeric systems is becoming increasingly viable.

While generating structural and thermodynamic properties for polymeric systems at equilibrium is relatively easy and employs the use of relatively short chains, simulating such systems under flow conditions is still under development. While there has been a large amount of effort dedicated to studying polymeric systems under shear flow [see, for example, Morriss *et al.* (1991); Daivis *et al.* (1992); Gray *et al.* (1995)], studying polymeric systems under elongational flow is still in the developmental stage. In the past several years, efforts have been made to simulate elongational flows using nonequilibrium molecular dynamics or nonequilibrium Monte Carlo (NEMC) algorithms [Kröger *et al.* (1997); Todd and Daivis (2000, 2003); Daivis and Todd (2006); Mavrantzas and Theodorou (1998); Mavrantzas and Öttinger (2002); Baig *et al.* (2005a, 2005b, 2006a, 2006b); Edwards *et al.* (2005, 2006)].

Typically, molecular dynamics methods are used when dynamic information, such as viscosity or diffusion coefficients, is needed. Given the large relaxation times of polymeric systems, simulation times on the order of tens of microseconds (as yet unobtainable) are often required to sample such properties. On the other hand, when static properties, such as internal conformation, density, or internal energy, are needed, Monte Carlo methods have emerged as a very useful tool for sampling efficiently such properties away from equilibrium for systems inaccessible to molecular dynamics [Pant and Theodorou (1995); Mavrantzas *et al.* (1999); Karayiannis *et al.* (2002)].

The critical development of the NEMC algorithm of Mavrantzas and Theodorou (1998) is the so-called "end-bridging" move [Pant and Theodorou (1995)], which allows chains to be broken and reformed according to a prescribed chemical potential. This introduces polydispersity into the system, in the sense that chain lengths are uniformly distributed within a predefined interval, and around a predefined average value. The computational efficiency of this algorithm was evaluated [Mavrantzas *et al.* (1999)] by

simulating n-alkane systems of up to 500 carbon atoms in length. It was concluded that the end-bridging algorithm was a least two orders of magnitude faster at equilibrating long-chain systems than any other molecular simulation method known at the time. Surprisingly, it was also shown that the algorithm became faster as the average length of the simulated chains increased. This is somewhat counterintuitive, but its explanation lies at the very heart of the algorithm: the longer the chains, the more options there are for them to break and recombine, and thus the greater the acceptance ratio of the end-bridging move.

The nonequilibrium version of this algorithm was developed for simulating oriented alkane melts under an applied orienting field. This was accomplished by defining two thermodynamic conjugate variables (the conformation tensor **c**, and the "orienting field" $\boldsymbol{\alpha}$) [Mavrantzas and Theodorou (1998)]. Later, a different method was used to develop a similar thermodynamic framework called GENERIC MC [Mavrantzas and Öttinger (2002)]. In this approach, the conjugate variables were introduced as proper Lagrange multipliers in the sense of a Legendre transformation, and a slightly different form for the orienting field $\boldsymbol{\alpha}$ was derived. This eliminated unwanted density fluctuations observed using the original form of the algorithm. In this section, the procedure of Mavrantzas and Öttinger (2002) is used to simulate systems with average chain lengths between 24 and 78 carbon atoms, at temperatures between 300 and 450 K, with applied orienting fields of varying strength.

## A. Simulation methodology

In a typical Monte Carlo algorithm, the initial configuration is defined by a set of Cartesian coordinates, which designate the position in space of every interaction site (or atom). The algorithm starts by randomly picking an atom or group of atoms and applying a random displacement to them. Then, the energy of the new system is evaluated, and the move is accepted or rejected with a probability that is dependent on temperature and the energy of the new system. The art in a Monte Carlo simulation lies in the choice of the type of move, as well as the proportion of moves attempted.

In the NEMC procedure used in this work, the following mix of attempted moves was used: reptations, 10%; rotations, 2%; flips, 6%; intrachain bridges, 32%; end bridges, 49%; volume fluctuations, 1%. These moves, as well as the choice of percentages from the total number of attempted moves, have been discussed in detail previously [Mavrantzas and Theodorou (1998); Mavrantzas *et al.* (1999)]. In the course of a simulation, the total number of chains, $N$, the total number of particles, $n$, the pressure, $p$, the temperature, $T$, and the spectrum of relative chemical potentials for different chain lengths, $\boldsymbol{\mu}^*$, are kept constant. This is called the $NnpT\boldsymbol{\mu}^*$ ensemble.

The force field used in this study is the Siepmann–Karaborni–Smit (SKS) potential model [Siepmann *et al.* (1993)], which was specifically parameterized to fit experimental thermodynamic data for alkane systems. In the SKS description, there are two types of interactions present in the system: bonded interactions and nonbonded interactions. The $CH_2$ groups that form the molecular chain are collapsed into a single interaction site, by using the so-called "united atom" approximation. This approach is possible given the relatively small size of the hydrogen atoms when compared to the carbon atoms. It is well known in the simulation community [Allen and Tildesley (1987)] that the computational expense is roughly proportional to the second power of the number of sites in the system. Strictly speaking, for a well-written Fortran program that uses optimal neighbor list algorithms, the computational expense is proportional to the number of particles multiplied by the number of neighbors per particle; for short ranged interactions, this is much

less than the square of the number of particles. By collapsing the $CH_2$ group into a single interaction site, the total number of particles in the system is reduced by a factor of 3, yielding a reduction of about one order of magnitude in the computational expense, without any loss in accuracy. From this point on, we will refer to the $CH_2$ sites as "atoms."

Typically, the total potential energy function in an atomistic level simulation is given as

$$U = U_{\text{bond}} + U_{\text{angle}} + U_{\text{torsion}} + U_{\text{nonbonded}}, \tag{8}$$

where $U_{\text{bond}}$, $U_{\text{angle}}$, and $U_{\text{torsion}}$, represent the bonded interactions, while $U_{\text{nonbonded}}$ represents the nonbonded interactions, which might include van der Waals terms, Coulombic terms, etc.

In Eq. (8), $U_{\text{bond}}$ represents the covalent bond-stretching interaction, which is typically represented by a harmonic spring with an equilibrium length, $r_0$. In the SKS description, this term is omitted and the covalent chemical bonds are modeled as rigid rods of 1.54 Å in length. $U_{\text{angle}}$ quantifies the angle bending interaction between two covalent bonds, and is given by a harmonic potential around an equilibrium value, $\theta_0$,

$$U_{\text{angle}} = \frac{1}{2}k_\theta(\theta - \theta_0)^2, \tag{9}$$

where $k_\theta$ is the harmonic spring constant. The torsional potential, $U_{\text{torsion}}$, is described by a function proposed by Jorgensen *et al.* (1984),

$$U_{\text{torsion}} = \sum_{k=0}^{3} a_k(\cos \Phi)^k, \tag{10}$$

where $a_k$ are constants and $\Phi$ the dihedral angle.

The nonbonded interactions are expressed in terms of a 12-6 Lennard-Jones (LJ) interaction potential,

$$U_{\text{nonbonded}} = 4\varepsilon\left[\left(\frac{\sigma}{r}\right)^{12} - \left(\frac{\sigma}{r}\right)^6\right]. \tag{11}$$

Nonbonded interactions occur between atoms on the same chain separated by more than three covalent bonds, and between all atoms belonging to separate chains. To reduce the computational cost, the nonbonded potential is truncated for distances greater than a specified cutoff radius, $r_{\text{cut}}$ [Allen and Tildesley (1987)]. In this study, a cutoff radius of $2.8\sigma$ was chosen [Mavrantzas and Theodorou (1998); Mavrantzas and Öttinger (2002)]. In Table I, the summary of the force field as well as the parameters for each type of interaction are presented.

With the interaction potentials defined, the total potential energy over the course of a simulation run can be calculated as an ensemble average over all configurations. Since the simulations are performed at constant temperature, there would be no change in the kinetic energy. Consequently, the change in the internal energy of an oriented configuration with respect to equilibrium will be given by the difference between the average total potential energy of the oriented system and the average total potential energy of the system at equilibrium

**TABLE I.** Details of the potential model used in the simulations.

| Type | Functional form | Parameters |
|------|-----------------|------------|
| $U_{bond}$ | Rigid $r = r_0$ | $r_0 = 1.54$ Å |
| $U_{angle}$ | $\frac{1}{2} k_\theta (\theta - \theta_0)^2$ | $k_\theta / k_B = 62,500$ K/rad$^2$ |
| | | $\theta_0 = 114°$ |
| $U_{torsion}$ | $\Sigma_{k=0}^{3} \alpha_k (\cos \Phi)^k$ | $a_0 / k_B = 1010$ K |
| | | $a_1 / k_B = 2019$ K |
| | | $a_2 / k_B = 136.4$ K |
| | | $a_3 / k_b = -3165$ K |
| $U_{nonbonded}$ | $4\varepsilon \left[ \left( \frac{\sigma}{r} \right)^{12} - \left( \frac{\sigma}{r} \right)^6 \right]$ | $\varepsilon_{CH_2} / k_B = \varepsilon_{CH_3} / k_B = 47$ K |
| | | $\sigma_{CH_2} = \sigma_{CH_3} = 3.93$ Å |

$$\frac{\Delta U}{N} = \frac{\langle U \rangle}{N} (\rho, T, \mathbf{c}) - \frac{\langle U \rangle}{N} (\rho, T, \boldsymbol{\delta}), \tag{12}$$

where $\boldsymbol{\delta}$ is the unit tensor. This equation will allow calculation of the change in the total internal energy, as well as calculation of individual contributions from the different types of interactions included in the potential model of Eq. (8).

## B. Thermodynamic considerations

In view of the definition of the conformation tensor expressed by Eq. (4), it is more convenient to work in terms of the normalized conformation tensor, $\widetilde{\mathbf{c}}$, which is defined as

$$\widetilde{\mathbf{c}} = 3 \frac{\mathbf{c}}{\langle R^2 \rangle_0} = \mu \mathbf{c}, \tag{13}$$

where $\langle R^2 \rangle_0$ is the mean-squared, end-to-end distance of a chain, taken as an ensemble average over all chains at equilibrium, and $\mu$ the normalization factor. Clearly, by definition, the normalized conformation tensor $\widetilde{\mathbf{c}}$ at equilibrium is equivalent to the unit tensor, $\boldsymbol{\delta}$. The Helmholtz free energy per chain of the oriented liquid is postulated to possess a direct dependence on $\widetilde{\mathbf{c}}$,

$$\frac{A}{N} = \frac{A}{N} (\rho, T, \widetilde{\mathbf{c}}). \tag{14}$$

The orienting field $\boldsymbol{\alpha}$ is introduced as the thermodynamic conjugate variable to $\widetilde{\mathbf{c}}$,

$$\alpha_{\gamma\delta} = \frac{1}{k_B T} \left[ \frac{\partial}{\partial \widetilde{c}_{\gamma\delta}} \frac{A}{N} (\rho, T, \widetilde{\mathbf{c}}) \right]_{T, \rho, \widetilde{c}_{[\gamma\delta]}}. \tag{15}$$

This expression is entirely congruent with the concept of a Legendre transformation in equilibrium thermodynamics. In this equation, the orienting field $\boldsymbol{\alpha}$ is defined at constant density. However, the NEMC simulations are performed at constant pressure; therefore, it is more useful to define a new thermodynamic potential function (the Gibbs free energy function, $G$) by performing a Legendre transformation of the Helmholtz free energy with respect to $V/N$ and $\widetilde{\mathbf{c}}$,

**TABLE II.** Molecular aspects of the simulated systems.

| System | $N$ (Total number of chains) | $n$ (Total number of particles) | $MWDI$ (Distribution interval) | $PI$ (Polydispersity index) |
|--------|---------|---------|---------|---------|
| $C_{24}$ | 100 | 2400 | 12–36 | 1.0902 |
| $C_{36}$ | 64 | 2304 | 18–54 | 1.0953 |
| $C_{50}$ | 49 | 2450 | 25–75 | 1.0866 |
| $C_{78}$ | 40 | 3120 | 39–117 | 1.0854 |

$$\frac{G}{N}(p,T,\boldsymbol{\alpha}) = \frac{A}{N}(\rho,T,\widetilde{\mathbf{c}}) + \frac{p}{\rho}\frac{M}{N_A} - k_B T \boldsymbol{\alpha}{:}\widetilde{\mathbf{c}}. \tag{16}$$

In this expression, $M$ is the number average molecular weight of the chains, $N_A$ is Avogadro's number, and $k_B T \boldsymbol{\alpha}{:}\widetilde{\mathbf{c}}$ accounts for the energy of the imposed orienting field. It immediately follows that

$$\widetilde{c}_{\gamma\delta} = -\frac{1}{k_B T}\left[\frac{\partial}{\partial \alpha_{\gamma\delta}}\frac{G}{N}(p,T,\boldsymbol{\alpha})\right]_{T,p,\alpha_{[\gamma\delta]}}, \tag{17}$$

where $\alpha_{[\gamma\delta]}$ represents all components of the orienting field tensor except $\alpha_{\gamma\delta}$.

The ultimate goal in these simulations is to evaluate the change in the Helmholtz free energy with respect to the quiescent melt. By performing simulations with applied orienting fields of varying strength, the conformation tensor can be calculated, and the Gibbs free energy change is evaluated via a thermodynamic integration as

$$\frac{\Delta G}{N} \equiv \frac{G}{N} - \frac{G_0}{N} \equiv \frac{G}{N}(p,T,\boldsymbol{\alpha}) - \frac{G}{N}(p,T,\mathbf{0}) = -k_B T\left[\sum_{\gamma}\sum_{\delta}\int_0^{\alpha_{\gamma\delta}}\widetilde{c}_{\gamma\delta}\mathrm{d}\alpha_{\gamma\delta}\right]_{T,p,\alpha_{[\gamma\delta]}}. \tag{18}$$

Combining Eqs. (16) and (18), an expression is obtained for the change in Helmholtz free energy/chain as

$$\frac{\Delta A}{N} \equiv \frac{A}{N} - \frac{A_0}{N} = -k_B T\left[\sum_{\gamma}\sum_{\delta}\int_0^{\alpha_{\gamma\delta}}\widetilde{c}_{\gamma\delta}\mathrm{d}\alpha_{\gamma\delta}\right]_{T,p,\alpha_{[\gamma\delta]}} - p\frac{M}{N_A}\left(\frac{1}{\rho} - \frac{1}{\rho_0}\right) + k_B T \boldsymbol{\alpha}{:}\widetilde{\mathbf{c}}. \tag{19}$$

## C. System details

Using the Monte Carlo procedure described above, four different systems of linear alkane chains of varying average molecular weight were considered. The average chain lengths for the four systems were equal to 24, 36, 50, and 78 carbon atoms. From this point onward, these systems will be referred to as $C_{24}$, $C_{36}$, $C_{50}$, and $C_{78}$, respectively. One of the most appealing aspects of the end-bridging algorithm is the ability to generate polydisperse systems of controlled molecular weight distribution. As described previously [Mavrantzas and Theodorou (1998); Mavrantzas and Öttinger (2002)], the molecular weights for the systems considered in this study were uniformly distributed between $0.5 \cdot \langle MW \rangle$ and $1.5 \cdot \langle MW \rangle$, corresponding to polydispersity indices of about 1.09—see Table II. For example, in the $C_{24}$ system, the chain lengths were uniformly distributed

between 12 and 36 carbon atoms. For all systems, the input configurations were initially well equilibrated using an equilibrium molecular dynamics code, DL_POLY_2.0 [Smith and Forester (1996)]. The equilibration was performed at a constant temperature of 500 K under constant pressure conditions (1 atm) for a period of 2.5 ns. The well-equilibrated configurations thus obtained were then used as input into the NEMC code as initial configurations for each run. The applied orienting field $\boldsymbol{\alpha}$ employed was in the form proposed by Mavrantzas and Öttinger (2002), and corresponds to a uniaxial extensional field applied in the $x$ direction,

$$\boldsymbol{\alpha} = \begin{pmatrix} \alpha_{xx} & 0 & 0 \\ 0 & -\alpha_{xx}/2 & 0 \\ 0 & 0 & -\alpha_{xx}/2 \end{pmatrix}. \tag{20}$$

Clearly, the magnitude of $\alpha_{xx}$ uniquely defines the "strength" of the orienting field. Therefore, $\alpha_{xx}$ will be used from this point on as a basis to relate various physical properties to the strength of the orienting field. For all systems, simulations were carried out with $\alpha_{xx}$ ranging from 0.0 (equilibrium case) to 0.7 in 0.1 increments. To investigate temperature effects, separate runs were performed at 300, 350, 400, and 450 K for all systems and field strengths considered. In Table II, the molecular aspects of the systems considered are presented in terms of average chain lengths, chain length distribution intervals, numbers of chains, numbers of atoms, and polydispersity indices.

## IV. RESULTS

### A. Equilibrium simulation results

Perhaps the most useful quantity that can be extracted from the equilibrium simulations of this study is the mean-squared, end-to-end distance, $\langle R^2 \rangle_0$. This quantity allows definition of two other useful parameters, which will be extensively used in this analysis: the conformation tensor normalization factor, $\mu$ [see Eq. (13)], and the overall chain spring constant, $K(T)$ [Dressler *et al.* (1999)]. These quantities are defined as

$$\mu = \frac{3}{\langle R^2 \rangle_0}, \tag{21}$$

$$K(T) = \frac{3k_B T}{\langle R^2 \rangle_0} = \mu k_B T. \tag{22}$$

As described by Beris and Edwards (1994), $K(T)$ originated from early statistical models of chain molecules, and was taken as a linear function of temperature (i.e., $\mu$ was taken as independent of temperature), under the assumption that the free energy of an ensemble of polymer chains was purely entropic in nature. Later, this assumption was removed, and an energetic component to the free energy was identified based upon the nonlinearity of $K(T)$ with respect to temperature [Dressler *et al.* (1999)]. Moreover, the same study identified a conformational contribution to the heat capacity, Eq. (7).

It is instructive to examine the behavior of the mean-squared, end-to-end distance with respect to chain length and temperature. Following a procedure similar to that of Mavrantzas and Theodorou (1998), $\langle R^2 \rangle_0$ can be calculated from a single simulation over the entire molecular weight distribution interval. In Fig. 1, $\langle R^2 \rangle_0$ is displayed for all four systems investigated at 450 K as a function of chain length. Notice the seamless overlap in the regions where chains having the same length are found in two adjacent systems. The scatter found in the $C_{78}$ system data is attributed to poor statistical sampling in the
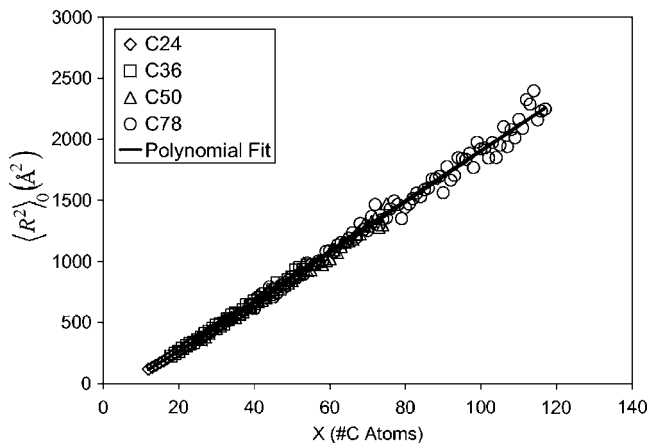
**FIG. 1.** Equilibrium mean-squared, end-to-end distance at $T = 450$ K.

calculation of the ensemble average. The $C_{78}$ system contained only 40 chains, while the molecular weight interval spanned 78 carbon atoms (39 on each side of 78). By contrast, the $C_{24}$ system contained 100 chains, while the molecular weight interval spanned 24 carbon atoms, resulting in much better statistics. Mavrantzas and Theodorou (1998) fitted the equilibrium mean-squared, end-to-end distance data to the polynomial expression,

$$C_X \equiv \frac{\langle R^2 \rangle_0}{(X-1)b^2} = \alpha_0 + \frac{\alpha_1}{X-1} + \frac{\alpha_2}{(X-1)^2} + \frac{\alpha_3}{(X-1)^3}, \qquad (23)$$

with very good results, where $C_X$ is the "characteristic ratio," $X$ the number of carbon atoms in a chain, $b$ the C–C bond length in Å (1.54 Å), and $\alpha_i$ ($i = 0-3$) fitting constants. In Table III, these parameters as derived from the equilibrium simulations in this study are presented, along with the published ones from the previous study [Mavrantzas and Theodorou (1998)]. However, in the previous study, only data from the $C_{24}$ and $C_{78}$ systems were generated at a single temperature (450 K). In the present study, the $\langle R^2 \rangle_0$ data in the overlapping regions were averaged, and the average value was considered in the polynomial fitting. As pointed out by Mavrantzas and Theodorou (1998), $\alpha_0$ is the characteristic ratio at infinite chain length, $C_\infty$. The value reported in this study at 400 K is slightly lower than the one previously reported, and closer to $C_\infty = 7.8 \pm 0.4$ measured for polyethylene using neutron diffraction at 413 K [Horton *et al.* (1989); Fetters *et al.* (1997)].

**TABLE III.** Characteristic ratio fitting parameters at various temperatures. The asterisk denotes the parameters of Mavrantzas and Theodorou (1998) at $T = 450$ K.

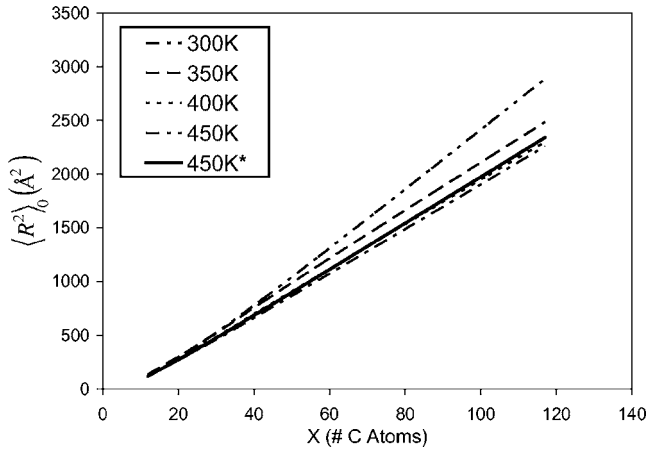| Temperature | $\alpha_0$ | $\alpha_1$ | $\alpha_2$ | $\alpha_3$ |
|:-----------:|:----------:|:----------:|:----------:|:----------:|
| 450 K  | 8.8  | −77.9  | 521.9   | −2141.8 |
| 400 K  | 8.6  | −30.6  | −681.7  | 6030.1  |
| 350 K  | 9.2  | −9.3   | −1573.4 | 13064.9 |
| 300 K  | 11.9 | −183.7 | 2022.2  | −9320.5 |
| 450 K* | 9.1  | −75.2  | 315.7   | −500.3  |

**FIG. 2.** $\langle R^2 \rangle_0$ polynomial fits using Eq. (23) and the fitting parameters in Table III.

In Fig. 2, the results of the polynomial fits in terms of $\langle R^2 \rangle_0$ are plotted against chain length, $X$. We observe a very close agreement between the new results and those published previously. Furthermore, we observe a strong temperature effect on $\langle R^2 \rangle_0$ in the sense that as the temperature is lowered, $\langle R^2 \rangle_0$ increases. In most prior cases, this behavior was overlooked, and $\langle R^2 \rangle_0$ (or $\mu = 3/\langle R^2 \rangle_0$) was taken as independent of temperature, with some exceptions [Gupta and Metzner (1982); Dressler *et al.* (1999); Dressler (2000)]. The temperature dependence of $\mu$ was introduced by Gupta and Metzner (1982) through an extra term in their constitutive equation to account for nonisothermal effects. Under isothermal conditions, their model reduced to the Upper-Convected Maxwell Model. In contrast to the new simulation results, they reported an increase in $\langle R^2 \rangle_0$ with increasing temperature. However, it is presently shown that the functional form of $\mu$,

$$\mu = \nu T^{-(B+1)}, \tag{24}$$

where $\nu$ and $B$ are constant parameters, fitted the simulation data very well, except for the contrary behavior, mentioned above. Gupta and Metzner pointed out that $B$ is a number greater than $-1$, and $\nu$ is a positive constant. With $B$ greater than $-1$, $\mu$ will decrease with decreasing temperature, and $\langle R^2 \rangle_0$ will increase with temperature. The simulation results imply the opposite effect—see Fig. 2. However, the simulation results are in good quantitative agreement with data reported by Ciferri *et al.* (1961) for cross-linked polyethylene at 140 °C ($\partial \ln \langle R^2 \rangle_0 / \partial T = -1.1 \cdot 10^{-3}$ K$^{-1}$). They are also consistent with recent end-bridging MC simulations of a bulk and grafted amorphous PE system above and below its glass transition temperature [Alexiadis *et al.* (2007)]. By combining Eqs. (21) and (24), and then taking the derivative with respect to temperature, one obtains $B = -1.45$ from the data of Ciferri *et al.* (1961).

In Fig. 3, the temperature exponent $B$ resulting from fitting the data in Fig. 2 is plotted against chain length. It is evident that the temperature exponent extrapolates to $B = -1.00$ at zero chain length (i.e., no temperature dependence of $\mu$). The temperature exponent $B$ decreases with increasing chain length, and seems to asymptote to a constant value of $-1.62$ for very high chain lengths, not too far from the reported experimental value of Ciferri *et al.* (1961).
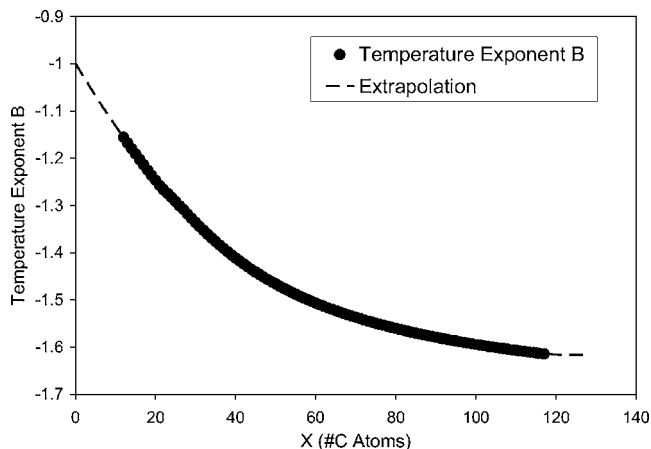
**FIG. 3.** The temperature exponent $B$ with respect to chain length.

## B. Nonequilibrium simulation results

The equilibrium simulations provided two very important pieces of information that were useful in the next step of the analysis. First, they provided the normalizing coefficient $\mu$ and its temperature dependence, which will be used further for calculating the normalized conformation tensor for the oriented systems. Second, they provided the reference for calculating the change in internal energy of the oriented structures according to Eq. (12). Furthermore, it was shown that $\langle R^2 \rangle_0$ is indeed dependent on temperature.

The model systems were examined under the application of a finite orienting field; however, it was first necessary to make sure that there were no system-size effects influencing the results. It is well known that highly oriented polymer chains may develop unphysical artifacts introduced by interactions between extended images of the same chain. These artifacts are known to induce a "premature crystallization" phenomenon, and can be eliminated by increasing the size of the simulation box [Baig *et al.* (2006a)]. To test the system-size effect, the $C_{78}$ system was used since it is the most vulnerable to such artifacts as it had the largest extended chain length. Additional systems were generated which were two and four times larger than the original system (containing 6240 and 12480 atoms, respectively). The evolution of all three systems was monitored under applied orienting fields up to and including $\alpha_{xx} = 0.7$ at $T = 450$ K. All relevant quantities (energies, conformation tensor, end-to-end vector auto-correlation functions) were examined for symptoms of premature crystallization, and it was concluded that, within statistical uncertainty, all of these quantities converged to the same value for a sufficiently large number of iterations. The reason for this is that the end-bridging move cleaves the longer chains at a high frequency, drastically reducing the possibility of an extended chain exiting opposite sides of the simulation cell at the same time. It is worth pointing out that the computational requirements of a typical Monte Carlo code are roughly proportional to the second power of the number of particles, $n^2$; therefore, by doubling the system size, it is necessary to quadruple the simulation time in order to generate the same statistics. Fortunately, for the range of field strengths employed in this study, larger systems were unnecessary.

The conformation tensor (or, more conveniently, its normalized form) was calculated for the oriented structures induced under various values of the applied field. By definition [see Eqs. (4) and (13)], the normalized conformation tensor $\tilde{\mathbf{c}}$ is symmetric and reduces to
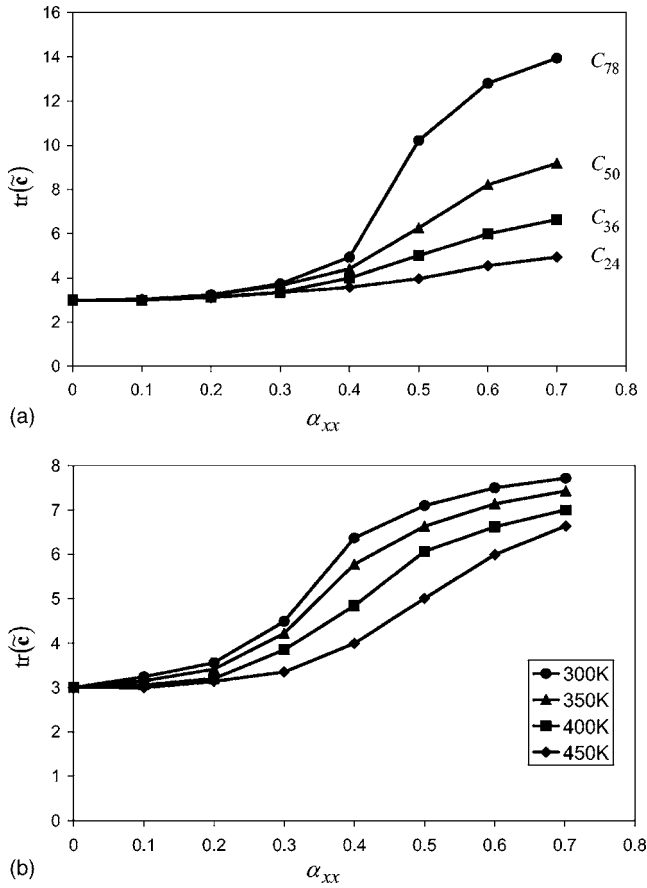
**FIG. 4.** Degree of extension vs. the strength of the orienting field: (a) the influence of molecular weight on conformation at $T=450$ K; (b) the influence of temperature on conformation for the $C_{36}$ system.

the unit tensor at equilibrium for any given temperature. When the orienting field is applied, the chains will adopt extended conformations, oriented on average in the direction of the extension, and $\widetilde{\mathbf{c}}$ will depart from its equilibrium value. In this situation, the degrees of extension and orientation will be uniquely described by the six independent components of $\widetilde{\mathbf{c}}$. Following the definition of the orienting field [Eqs. (15), (17), and (20)], one would expect the off-diagonal components of $\widetilde{\mathbf{c}}$ to be zero as well. Indeed, our simulations confirmed the diagonal form of $\widetilde{\mathbf{c}}$; therefore, the trace of $\widetilde{\mathbf{c}}$ can be used to quantify the degree of extension and orientation generated by the orienting field in the simulations.

In Fig. 4, the effects of molecular weight [Fig. 4(a)] and temperature [Fig. 4(b)] on conformation are examined as the strength of the orienting field is increased. As expected, there is an increase of the degree of orientation with molecular weight at a particular temperature, since the longer chains are capable of experiencing greater degrees of extension [Fig. 4(a)]. An increase in the degree of orientation with decreasing temperature at constant molecular weight is observed for $C_{36}$ in Fig. 4(b). This behavior matches the intuitive expectation that an increase in temperature augments the randomizing Brownian effect on the atomic particles.

Having performed calculations of the normalized conformation tensor for each value

of the molecular weight, temperature, and field strength, the Helmholtz free energy change relative to the unperturbed state, $\Delta A/N$, was calculated by performing a series of thermodynamic integrations according to Eq. (19). Such a methodology requires a series of simulation data for the conformation tensor $\widetilde{\mathbf{c}}$ at different values of the tensor $\boldsymbol{\alpha}$, since the integration should be performed along a path where only the value of one component of the tensor $\boldsymbol{\alpha}$ is varied, keeping the rest constant. The total number of simulation points to be collected is reduced by noting that the Helmholtz free energy is a state function, so that $\Delta A/N$ may be obtained by integrating over a suitable path that moves the system from a common initial state to the common final state. Since the tensor $\boldsymbol{\alpha}$ is postulated to possess the form of Eq. (20), one can obtain estimates of the free energy difference $\Delta A/N$ by assuming that only one of the three components $\alpha_{xx}$, $\alpha_{yy}$, and $\alpha_{zz}$ is independent, namely $\alpha_{xx}$, and the other two are constrained to be minus one half of that value (i.e., $\alpha_{yy} = \alpha_{zz} = -\alpha_{xx}/2$). Based on these remarks, $\Delta A/N$ is approximated as

$$\frac{\Delta A}{N} = -k_B T \int_0^{\alpha_{xx}} \left( \widetilde{c}_{xx} - \frac{\widetilde{c}_{yy}}{2} - \frac{\widetilde{c}_{zz}}{2} \right) d\alpha_{xx}. \tag{25}$$

This allows us to calculate $\Delta A/N$ by using the values of $\widetilde{c}_{xx}$, $\widetilde{c}_{yy}$, and $\widetilde{c}_{zz}$ obtained at progressively larger values of the field $\boldsymbol{\alpha}$, from the zero to the final state. However, as the applied field increases, $\widetilde{c}_{yy}$ and $\widetilde{c}_{zz}$ asymptote to zero, while tr $\widetilde{\mathbf{c}}$ rises dramatically. Under these conditions, $\widetilde{c}_{xx}$ is significantly larger than the other two diagonal components, and thus it represents essentially the entire contribution to the thermodynamic integration. Based on this, the variations in the compression directions were neglected in performing these integrations at high enough strain rates, which implies that the following equation was eventually used to calculate $\Delta A/N$:

$$\frac{\Delta A}{N} \cong -k_B T \int_0^{\alpha_{xx}} \widetilde{c}_{xx} d\alpha_{xx}. \tag{26}$$

Furthermore, the change in internal energy with respect to equilibrium, $\Delta U/N$, is readily available directly from the simulations, which allows for a direct comparison of the two quantities.

Figure 5 displays the molecular weight effect on $\Delta A/N$ and $\Delta U/N$ at 450 K [Fig. 5(a)], and the temperature effect on the same quantities for the $C_{36}$ system [Fig. 5(b)]. First, it is apparent that $\Delta A/N$ and $\Delta U/N$ are of about the same magnitude and of opposite sign for all of the cases considered. This suggests that the internal energy is a very important component of the free energy in the energetic balance of the system, at least at high field strengths. Furthermore, mirroring the results presented in Fig. 4, the same behavior is observed in terms of the free energy change as a function of both molecular weight and temperature. This is not at all surprising, since the change in free energy has an explicit dependence on the conformation tensor according to Eq. (19). It is well known that the free energy of a polymeric liquid depends on the degree of extension of the fluid's internal microstructure [Beris and Edwards (1994)], with the longer chain molecules being more highly extended for a specific value of $\alpha_{xx}$—see Fig. 4(a). The observed behavior of the free energy change with temperature at constant molecular weight in Fig. 5(b) is just as easily explained using the conclusion derived from Fig. 4(b): as temperature increases, the degree of orientation decreases due to Brownian effects, thus resulting in a lower value of the free energy at any particular value of $\alpha_{xx}$.

Examining the effect of the molecular weight on the change in internal energy, it is seen that, as the chain length increases, the decrease in internal energy for a given temperature and field strength is more pronounced. In these simulations, the ability exists
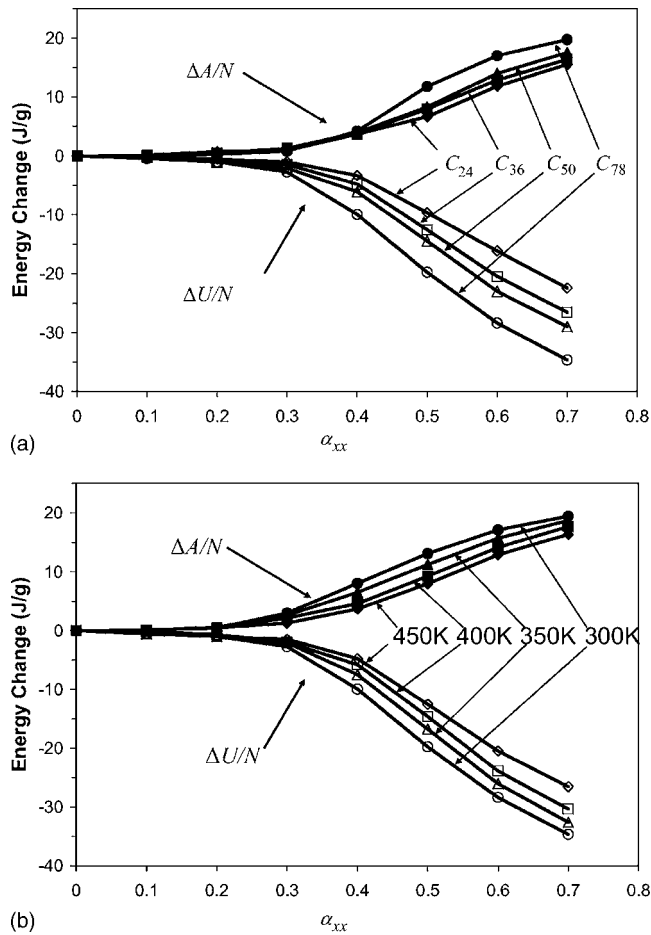
**FIG. 5.** The chain specific Helmholtz free energy and internal energy changes as functions of field strength: (a) the influence of molecular weight at $T=450$ K; (b) the influence of temperature for the $C_{36}$ system.

to evaluate the intermolecular and intramolecular contributions to the nonbonded energy separately. As discussed with respect to the next figure, the most important contributor to the total energy of the system is the intermolecular nonbonded energy. As the molecular weight increases, it is easier for the chains to establish favorable side-to-side interactions, generating a more pronounced decrease in the total internal energy. The temperature dependence of the internal energy [Fig. 5(b)] can be explained using the same line of thought. As the temperature decreases, the Brownian effect decreases as well, thus making it easier for the chains to align and develop the energetically favorable side-to-side interactions at a particular value of field strength.

In a previous study, Mavrantzas and Theodorou (1998) found that the energetic contribution to the free energy decreases with increasing molecular weight, in contrast to the behavior evident in Fig. 5(b). This discrepancy is due to the fact that Mavrantzas and Theodorou did not achieve high enough strain rates for the effect observed above to begin to manifest in the longer chain system ($C_{78}$). Thus, their conclusion with regard to the energetic component of the free energy (i.e., that it decreases with increasing chain
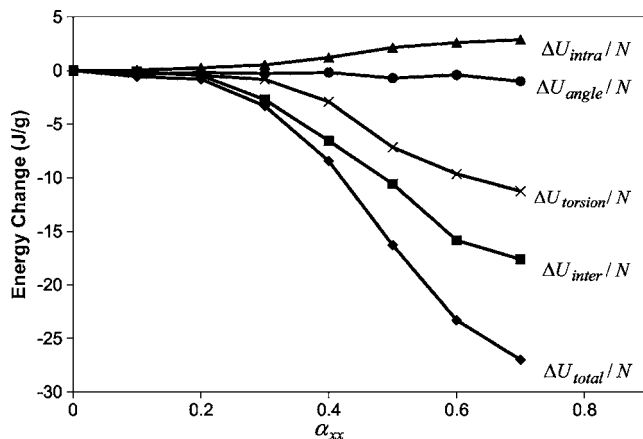
**FIG. 6.** Individual component contributions to the total internal energy change for the $C_{24}$ system at $T = 400$ K.

length) was not complete. However, they did state that if higher deformations had been achieved, then they would have expected to observe a more significant degree of energetic effects.

As mentioned earlier, it is possible to investigate the individual contribution of each type of interaction in Table I to the total internal energy. According to Eq. (8), the total potential energy is equal to the sum of all bonded and nonbonded interactions. In the simulations, the bonded interactions are represented by the angle bending and torsion interaction potentials, while the nonbonded interactions are represented by the 12–6 LJ pair interaction potential of Eq. (11). The nonbonded interactions can further be split into two distinct contributions: the intramolecular interactions, in which pairs of atoms belonging to the same chain, separated by more than three covalent bonds, interact through the LJ potential, and the intermolecular interactions, in which all pairs of atoms belonging to different chains interact through the same potential. This distinction is important because, as discussed relative to Fig. 6, the two components exhibit opposite behavior with respect to a change in the degree of orientation.

The potential energy change of the system relative to equilibrium can thus be written as

$$\frac{\Delta U_{\text{total}}}{N} = \frac{\Delta U_{\text{angle}}}{N} + \frac{\Delta U_{\text{torsion}}}{N} + \frac{\Delta U_{\text{intra}}}{N} + \frac{\Delta U_{\text{inter}}}{N}. \qquad (27)$$

In Fig. 6, the four energetic components on the right side of Eq. (27) are displayed for the $C_{24}$ system at $T = 400$ K as a function of $\alpha_{xx}$. As previously mentioned, it is clear from Fig. 6 that the two components of the nonbonded energy are of opposite sign and different in magnitude. The orienting field has almost no effect on the angle-bending energy, while the torsional energy decreases because the lower energy *trans* dihedral conformations of the extended chains are enhanced.

In the discussion of Sec. II, it was mentioned that, for a single isolated chain, the internal energy of the extended chain does not change significantly with the degree of extension, thus generating a purely entropic elastic response. This behavior can be explained upon close examination of Fig. 6. Unless extreme conditions are applied (i.e., the chain is fully extended, and additional energy is put into bending the valence angles), the angle energy does not change with the degree of extension. With increasing deformation,

the dihedral angles on the chain will gradually start to adopt the *trans* conformation (their lowest energy configuration), thus reducing the overall torsion energy. The intramolecular LJ energy will increase due to greater distances between the pairs of atoms in the extended configurations. It is clear from Fig. 6 that the changes in torsional and intramolecular potential energies are of about the same magnitude and opposite sign, thus essentially offsetting each other. From Fig. 6, it is evident that the most important contributor to the change in total energy is the intermolecular LJ energy. This is perhaps the most important conclusion from our simulations, and explains why the PEE assumption is not applicable to polymer melts. While the total internal energy of a single isolated chain may not change with extension (due to the two components discussed above offsetting each other), the internal energy of an ensemble of chains changes significantly due to favorable side-to-side interchain interactions, which lower the overall internal energy. Macroscopically, this will translate into additional energy being generated within the material, increasing the temperature of the fluid. Indeed, this aspect is confirmed by the experimental observations described by Ionescu *et al.* (2008), in which the calculated temperature increase due to deformation under the PEE assumption is under-predicted by up to 100% at the highest values of strain rate.

In Fig. 7(a), the free energy change calculated from the simulation via thermodynamic integration is compared with the same quantity as obtained by inserting the simulation results for $\widetilde{\mathbf{c}}$ (at any specific value of the field $\alpha$) in the free energy expression proposed by Booij (1984),

$$\frac{\Delta A}{N} = \frac{1}{2} k_B T (\mathrm{tr}\, \widetilde{\mathbf{c}} - 3) - \frac{1}{2} k_B T \ln \det \widetilde{\mathbf{c}}. \tag{28}$$

The agreement between the simulation data and the Booij free energy expression is excellent for all values of the molecular weight and temperature. In a previous study of polyethylene chains, Mavrantzas and Öttinger (2002) reported that the two free energies, one from the thermodynamic integration and the other from Eq. (28), differed increasingly as $\alpha_{xx}$ increased. However, this discrepancy was due to the fact that the maximum field strength ($\alpha_{xx} = 0.3$ instead of 0.7) led to an increase in absolute error, due to diminishing computational time, which was not considered as significant at the higher field values viewed from a relative error basis. Note that the values of the free energy for all common values (i.e., $0 \leq \alpha_{xx} \leq 0.3$) reported in both papers are equivalent.

The agreement between the free energies above provides an indication that it is possible to calculate the heat capacity from Eq. (7). In Figs. 7(b) and 7(c), the corresponding prediction for the conformational contribution to the dimensionless heat capacity is displayed [Dressler *et al.* (1999)], as computed according to the Booij expression, Eq. (28). Note that the effect of orientation is to reduce the heat capacity, as expected. This is because the intermolecular side-to-side interactions in the oriented melt result in a reduced internal energy relative to the equilibrium system configuration, and the difference between the two increases as temperature decreases. Therefore, the heat capacity must be reduced as well, since, by definition [see Eq. (6)], this is the partial derivative of $\hat{U}$ with respect to $T$; i.e., as evident from Fig. 4(b), decreasing temperature increases the degree of orientation (a smaller Brownian effect), which must then decrease the heat capacity. Hence, as temperature is decreased [Fig. 7(c)], the heat capacity decreases as well. Figure 7(b) also offers consistent evidence, since the heat capacity decreases with molecular weight, it must be greatly affected by the degree of orientation—see Fig. 4(a).
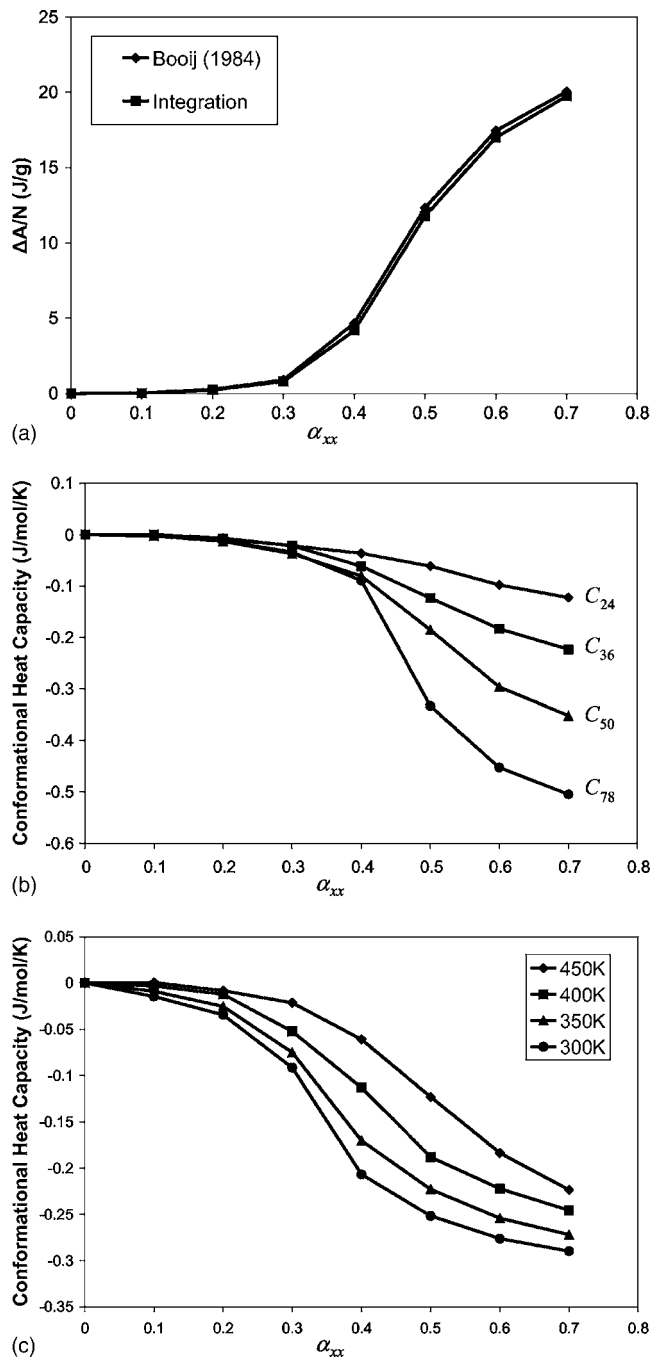
**FIG. 7.** The Helmholtz free energy vs. field strength computed using the Booij free energy expression [Eq. (28), labeled "Booij"] and via thermodynamic integration [Eq. (26)] (a), and the conformational contribution to the heat capacity as a function of field strength (b), and temperature (c).

## V. CONCLUSIONS

The most important result of this work is that the response of short, unentangled PE liquids to an elongational flow field is not purely entropic; a significant energetic com-

ponent appears at high field strengths due to the development of favorable lateral inter-molecular interactions between oriented chain segments. This was observed to be the case not only for the shorter chains (such as $C_{24}$), but also for the longer chains (such as $C_{78}$). This result supports recent experimental and finite element-based rheological data for a PE melt in a semihyperbolically converging die [Ionescu *et al.* (2008)], where a standard form of the temperature evolution equation arising from the concept of purely entropic elasticity was demonstrated to be inadequate to describe nonisothermal flow under a high degree of deformation.

Simulation results for the Helmholtz free energy of the elongated PE systems were compared to the analytical expression proposed by Booij (1984) involving only two of the three invariants of the conformation tensor, the trace and the determinant. Although not identical, the agreement between the two sets of data was quite satisfactory over the entire range of conformation tensor values.

We also calculated the chain spring constant $K(T)$ and, in contrast to what has often been assumed, this was found not to be a linear function of temperature. Computed values of the temperature exponent $B$ quantifying the nonlinear relationship between $K$ and $T$ as a function of chain length were found to be in very good agreement with experimental measurements and previous simulation results.

## ACKNOWLEDGMENTS

## References

Alexiadis, O., V. G. Mavrantzas, R. Khare, J. Beckers, and A. R. C. Baljon, "End-bridging Monte Carlo simulation of bulk and grafted amorphous polyethylene above and below the glass transition," Macromolecules (in press).

Allen, M. P., and D. J. Tildesley, *Computer Simulation of Liquids* (Oxford University Press, Oxford, 1987).

Astarita, G., "Thermodynamics of dissipative materials with entropic elasticity," Polym. Eng. Sci. **14**, 730–733 (1974).

Astarita, G., and G. C. Sarti, "The dissipative mechanism in flowing polymers: Theory and experiments," J. Non-Newtonian Fluid Mech. **1**, 39–50 (1976a).

Astarita, G., and G. C. Sarti, "An approach to thermodynamics of polymer flow based on internal state variables," Polym. Eng. Sci. **16**, 490–495 (1976b).

Baig, C., B. J. Edwards, D. J. Keffer, and H. D. Cochran, "A proper approach for nonequilibrium molecular dynamics simulations of planar elongational flow," J. Chem. Phys. **122**, 114103 (2005a).

Baig, C., B. J. Edwards, D. J. Keffer, and H. D. Cochran, "Rheological and structural studies of liquid decane, hexadecane, and tetracosane under planar elongational flow using nonequilibrium molecular-dynamics simulations," J. Chem. Phys. **122**, 184906 (2005b).

Baig, C., B. J. Edwards, D. J. Keffer, H. D. Cochran, and V. A. Harmandaris, "Rheological and structural studies of linear polyethylene melts under planar elongational flow using nonequilibrium molecular dynamics simulations," J. Chem. Phys. **124**, 084902 (2006a).

Baig, C., B. Jiang, B. J. Edwards, D. J. Keffer, and H. D. Cochran, "A comparison of simple rheological models

and simulation data of n-hexadecane under shear and elongational flow," J. Rheol. **50**, 625–640 (2006b).

Baig, C., and V. G. Mavrantzas, "Thermodynamically guided nonequilibrium Monte Carlo for generating realistic shear flows in polymeric systems," Phys. Rev. Lett. **99**, 257801 (2007).

Bedrov, D., and G. D. Smith, "The role of local conformations in the stretching of a poly(ethylene oxide) chain in solution," J. Chem. Phys. **118**, 6656–6663 (2003).

Beris, A. N., and B. J. Edwards, "Poisson bracket formulation of incompressible flow equations in continuum mechanics," J. Rheol. **34**, 55–78 (1990a).

Beris, A. N., and B. J. Edwards, "Poisson bracket formulation of viscoelastic flow equations of differential type: A unified approach," J. Rheol. **34**, 503–538 (1990b).

Beris, A. N., and B. J. Edwards, *Thermodynamics of Flowing Systems* (Oxford University Press, Oxford, 1994).

Bernardin, F. E., III, and G. C. Rutledge, "Semi-grand canonical Monte Carlo (SGMC) simulations to interpret experimental data on processed polymer melts and glasses," Macromolecules **40**, 4691–4702 (2007).

Booij, H. C., "The energy storage in the Rouse model in an arbitrary flow field," J. Chem. Phys. **80**, 4571–4572 (1984).

Ciferri, A., C. A. J. Hoeve, and P. J. Flory, "Stress-temperature coefficients of polymer networks and conformational energy of polymer chains," J. Am. Chem. Soc. **83**, 1015–1022 (1961).

Daivis, P. J., D. J. Evans, and G. P. Morriss, "Computer-simulation study of the comparative rheology of branched and linear alkanes," J. Chem. Phys. **97**, 616–627 (1992).

Daivis, P. J., and B. J. Todd, "A simple, direct derivation and proof of the validity of the SLLOD equations of motion for generalized homogeneous flows," J. Chem. Phys. **124**, 194103 (2006).

Dressler, M., "The dynamical theory of non-isothermal polymeric materials," Ph.D. Dissertation, ETH, Zurich (2000).

Dressler, M., B. J. Edwards, and H. C. Ottinger, "Macroscopic thermodynamics of flowing polymeric liquids," Rheol. Acta **38**, 117–136 (1999).

Edwards, B. J., C. Baig, and D. J. Keffer, "An examination of the validity of nonequilibrium molecular-dynamics simulation algorithms for arbitrary steady-state flows," J. Chem. Phys. **123**, 114106 (2005).

Edwards, B. J., C. Baig, and D. J. Keffer, "A validation of the p-SLLOD equations of motion for homogeneous steady-state flows," J. Chem. Phys. **124**, 194104 (2006).

Fetters, L. J., W. W. Graessley, R. Krishnamoorti, and D. J. Lohse, "Melt chain dimensions of poly(ethylene-1-butene) copolymers via small angle neutron scattering," Macromolecules **30**, 4973–4977 (1997).

Flory, P. J., *Principles of Polymer Chemistry* (Cornell University Press, Ithaca, New York, 1953).

Gray, R. A., P. B. Warren, S. Chynoweth, Y. Michopoulos, and G. S. Pawley, "Crystallization of molecular liquids through shear-induced nucleation," Proc. R. Soc. London, Ser. A **448**, 113–120 (1995).

Gupta, R. K., and A. B. Metzner, "Modeling of non-isothermal polymer processes," J. Rheol. **26**, 181–198 (1982).

Horton, J. C., G. L. Squires, A. T. Boothroyd, L. J. Fetters, A. R. Rennie, C. J. Glinka, and R. A. Robinson, "Small-angle neutron scattering from star-branched polymers in the molten state," Macromolecules **22**, 681–686 (1989).

Ionescu, T. C., C. Baig, B. J. Edwards, D. J. Keffer, and A. Habenschuss, "Structure formation under steady-state isothermal planar elongational flow of n-eicosane: A comparison between simulation and experiment," Phys. Rev. Lett. **96**, 037802 (2006).

Ionescu, T., B. J. Edwards, D. J. Keffer, and V. G. Mavrantzas, "Energetic and entropic elasticity of nonisothermal flowing polymers: Experiment, theory, and simulation," J. Rheol. **52**, 105–140 (2008).

Jorgensen, W. L., J. D. Madura, and C. J. Swenson, "Optimized intermolecular potential functions for liquid hydrocarbons," J. Am. Chem. Soc. **106**, 6638–6646 (1984).

Karayiannis, N. C., V. G. Mavrantzas, and D. N. Theodorou, "A novel Monte Carlo scheme for the rapid equilibration of atomistic model polymer systems of precisely defined molecular architecture," Phys. Rev. Lett. **88**, 105503 (2002).

Kröger, M., C. Luap, and R. Muller, "Polymer melts under uniaxial elongational flow: Stress-optical behavior from experiments and nonequilibrium molecular dynamics computer simulations," Macromolecules **30**, 526–539 (1997).

Lu, Z. Y., W. Nowak, G. R. Lee, P. E. Marszalek, and W. T. Yang, "Elastic properties of single amylose chains

in water: A quantum mechanical and AFM study," J. Am. Chem. Soc. **126**, 9033–9041 (2004).

Mavrantzas, V. G., and D. N. Theodorou, "Atomistic simulation of polymer melt elasticity: Calculation of the free energy of an oriented polymer melt," Macromolecules **31**, 6310–6332 (1998).

Mavrantzas, V. G., and D. N. Theodorou, "Atomistic Monte Carlo simulation of steady-state uniaxial, elongational flow of long-chain polyethylene melts: Dependence of the melt degree of orientation on stress, molecular length and elongational strain rate," Macromol. Theory Simul. **9**, 500–515 (2000).

Mavrantzas, V. G., T. D. Boone, E. Zervopoulou, and D. N. Theodorou, "End-bridging Monte Carlo: A fast algorithm for atomistic simulation of condensed phases of long polymer chains," Macromolecules **32**, 5072–5096 (1999).

Mavrantzas, V. G., and H. C. Öttinger, "Atomistic Monte Carlo simulations of polymer melt elasticity: Their nonequilibrium thermodynamics GENERIC formulation in a generalized canonical ensemble," Macromolecules **35**, 960–975 (2002).

Morriss, G. P., P. J. Daivis, and D. J. Evans, "The rheology of normal alkanes: Decane and eicosane," J. Chem. Phys. **94**, 7420–7433 (1991).

Nakajima, K., H. Watabe, and T. Nishi, "Single polymer chain rubber elasticity investigated by atomic force microscopy," Polymer **47**, 2505–2510 (2006).

Ortiz, C., and G. Hadziioannou, "Entropic elasticity of single polymer chains of poly(methacrylic acid) measured by atomic force microscopy," Macromolecules **32**, 780–787 (1999).

Öttinger, H. C., *Beyond Equilibrium Thermodynamics* (Wiley, NJ, 2005).

Pant, P. V. K., and D. N. Theodorou, "Variable connectivity method for the atomistic Monte Carlo simulation of polydisperse polymer melts," Macromolecules **28**, 7224–7234 (1995).

Sarti, G. C., and N. Esposito, "Testing thermodynamic constitutive equations for polymers by adiabatic deformation experiments," J. Non-Newtonian Fluid Mech. **3**, 65–76 (1977).

Shi, W. Q., Y. H. Zhang, C. J. Liu, Z. Q. Wang, X. Zhang, and Y. M. Chen, "Toward understanding the effect of substitutes and solvents on entropic and enthalpic elasticity of single dendronized copolymers," Polymer **47**, 2499–2504 (2006).

Siepmann, J. I., S. Karaborni, and B. Smit, "Simulating the critical behavior of complex fluids," Nature (London) **365**, 330–332 (1993).

Smith, J. S., D. Bedrov, G. D. Smith, and E. M. Kober, "Thermodynamic and conformational changes upon stretching a poly(dimethylsiloxane) chain in the melt," Macromolecules **38**, 8101–8107 (2005).

Smith, W., and T. R. Forester, "DL_POLY_2.0: A general purpose parallel molecular dynamics simulation package," J. Mol. Graphics **14**, 136–141 (1996).

Todd, B. D., and P. J. Daivis, "The stability of nonequilibrium molecular dynamics simulations of elongational flows," J. Chem. Phys. **112**, 40–46 (2000).

Todd, B. D., and P. J. Daivis, "Nonlinear shear and elongational rheology of model polymer melts by nonequilibrium molecular dynamics," J. Non-Newtonian Fluid Mech. **111**, 1–18 (2003).

Treloar, L. R. G., *The Physics of Rubber Elasticity*, 3rd ed. (Clarendon, Oxford, United Kingdom, 1975).